Journal of Materials Chemistry A

COMMUNICATION

Cite this: J. Mater. Chem. A, 2018, 6, 845

Received 6th October 2017
Accepted 13th December 2017

DOI: 10.1039/c7ta08814k

rsc.li/materials-a

A phenol-formaldehyde polymeric network to generate organic aerogels: synthesis, physicochemical characteristics and potential applications†

Halyna Zubyk,[a] Olena Mykhailiv,[a] Anthony N. Papathanassiou,[b] Bogdan Sulikowski,[c] Elzbieta Zambrzycka-Szelewa,[a] Michael Bratychak[d] and Marta E. Plonska-Brzezinska *[a]

In this study, phenol-formaldehyde (PhF) resins, bisphenol A diglycidyl ether and 4-vinylpyridine were used for the preparation of two organic aerogels (AGs). The data showed that the organic AGs exhibited porous and functionalized structures resulting in efficient Cu(II) and Mn(II) ion removal from water sources. The AGs showed also fairly good sorption properties towards organic solvents and dyes. Combined complex permittivity and ac electrical conductivity measurements sense structural changes, indicating that AGs can also be promising sensors for the interaction of fluids interpenetrating their porous system.

Interest in aerogels (AGs) has surged in recent years due to their applications ranging from medical devices, personal care products, sensing, catalysis, separation to environmental remediation.[1–8] AGs are nanostructured materials consisting of nanoscale building blocks forming a porous three-dimensional (3D) network of components cross-linked by covalent bonding or physical interactions. They are synthetic or natural materials in which the liquid is replaced by gas, leaving the pores without destroying the porous structure.[1,9] Due to high porosity, they have unique physical and chemical properties, such as ultra-low thermal conductivity, high permittivity, high specific surface area and high permeability of sunlight.[10–12] Because of these unique properties and structures, they are recognized as next-generation materials. At the end of the 1980s, Pekala and coworkers for the first time used an organic polymer (resorcinol–formaldehyde) to create a polymer AG.[11] Since then, rapid development of the family of organic AGs has been observed, including aero-sponge-like materials containing polyimide, phenol-formaldehyde, poly(vinyl chloride), poly(vinyl alcohol), cellulose, cyclodextrin and resol derivatives.[3,7,9,13–17]

Here, we describe the preparation of two phenol-formaldehyde-based AGs containing modified phenol-formaldehyde (PhF) resins (Scheme 1). This study presents the example of PhF resin-based AGs applied for environmental remediation, removal of organic molecules and heavy metal ion sorption from water sources. Recently porous materials have drawn significant attention as sorbents in water treatment due to simple and fast processes.[18] Several techniques have been adopted for water treatment, such as adsorption,[19–21] membrane filtration,[22] ion exchange,[23] capacitive deionization,[24] electrosorption,[25,26] phytoremediation,[27] and catalysis.[28,29]

To the best of our knowledge, there is still limited knowledge regarding the application of AGs in removing organic molecules and heavy metal ions. In our study, we suggest using the resins

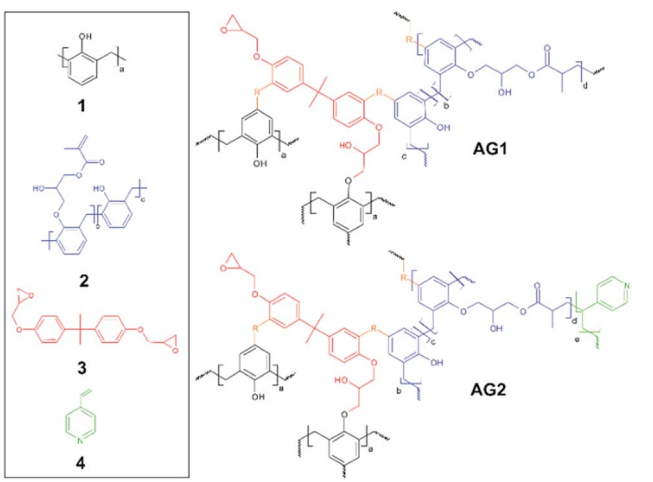

Scheme 1 Structure scheme of the products: (1) PhF resin, (2) PhF resin with methacrylate groups, (3) bisphenol A diglycidyl ether, and (4) 4-vinylpyridine and the possible fragments of crosslinked structures of AG1 and AG2.

[a]Institute of Chemistry, University of Bialystok, Ciolkowskiego 1K, 15-245 Bialystok, Poland. E-mail: mplonska@uwb.edu.pl

[b]National and Kaposdistrian University of Athens, Physics Department, Panepistimiopolis, GR 15784 Athens, Greece

[c]Jerzy Haber Institute of Catalysis and Surface Chemistry, Polish Academy of Sciences, Niezapominajek 8, 30-239 Cracow, Poland

[d]Lviv Polytechnic National University, Bandera 12, 79013 Lviv, Ukraine

† Electronic supplementary information (ESI) available. See DOI: 10.1039/c7ta08814k

which after oligomerization can be easily converted into organic multi-functional AGs (Scheme 1 and Fig. 1). We used PhF resins, which are well known and available products with excellent thermal resistance properties, and they are widely used as polymer composites and protective coatings.[1,30,31] PhF resins were synthesized according to a known method with slight modifications, and they were also used for formation of organic AGs.[32] Using **1**, **2** and **3** for the formation of the oligomer structures, a lot of hydroxyl, phenyl and epoxy groups were introduced into the polymeric network, leading to increased hydrophilicity and reactivity. The latter property also makes it possible further modification of the polymer chain and enables control of the hydrophilic/hydrophobic properties of the materials. This is a key parameter affecting the physicochemical properties of HGs and AGs and enabling their further applications.

The compositions of resins used for the preparation of organic AGs (AG1 and AG2) are presented in Table S1.† The key to the successful synthesis of these resins is a judicious selection of monomers and a hardening component. In the ESI† we present only the optimal conditions of the procedure established by our group for the AG formation, taking into account mainly the structural porosity and density of final materials. Briefly, two mixtures of PhF-based resins were synthesized using PhF resin (**1**), PhF resin with methacrylate groups (**2**), bisphenol A glycidyl ether (**3**) and/or 4-vinylpyridine (**4**). Resin 1 was composed of PhF resin (38% mass), PhF resin with methacrylate groups (26% mass), bisphenol A glycidyl ether (38% mass) and hexamethylenetetramine (12% mass) as a hardening component (Table SI1†). In the second case, 4-vinylpyridine was added (9% mass). The composition of the monomers used is summarized in Table S1.† For the formation of both resins 1/1.5 mL of 10% KOH in water and 1 mL of isopropanol were added. Upon heating at 80 °C within approximately 1 h we observed the formation of a gel network in both cases, as is shown in the schematic diagram of Panel 1 in Fig. 1. The resin gels were colored and homogenous, which proved the lack of phase separation (Fig. 1b and e, Panel 1). The gels were aged for 1 day leading to a strong and rigid polymer particle network. After thoroughly exchanging the mother liquid with the mixture of water/acetone and pristine acetone, as results of these processes, two organogels (OG1 and OG2) were obtained, which after supercritical drying (30 cycles in CO_2) formed the final AG1 and AG2 samples (Fig. 1 and Scheme 1). According to this reaction pathway, the pore sizes of AGs can be controlled by varying the polymerization time, in which the pre-oligomer formation reaction and oligomer particle growth occurred simultaneously. In this investigation, the aerogels were prepared without any microcracks in the gel network which was confirmed by scanning electron microscopy (SEM) (Fig. 1a and b in (P2)). The SEM images revealed 3D homogenous polymeric, porous networks of AG1 and AG2 with different diameters of particles depending on their chemical composition (Fig. 1(P2)). With an increase of magnification (Fig. 1(P2)), a small part of AGs can be observed consisting of spherical particles in both AGs. The average diameter of a particle in AG1 is 2–8 μm (Fig. 1(2a)), while in the AG2 skeleton, the particles formed a pearl necklace network with more homogenous structures and uniform sized particles (*ca.* 5 μm) (Fig. 1(2b)).

To confirm the formation of resins and their oligomerization, Attenuated Total Reflection Fourier Transform Infrared (ATR-FTIR) spectroscopy measurements were performed (Fig. 2). In this work only the changes in the ATR-IR spectra which are essential for the formation of the polymeric networks are underlined. The broad intense band at about 3600–3100 cm^{-1} represents the stretching vibrations of H-bonded hydroxyl (O–H) groups of alcoholic and phenolic resins (Fig. 2a, b, and d–f). Therefore, this wide band may also be attributed to self-H-bonds and N from pyridine rings and other H atoms from the polymeric network. The weak C–H vibration bands at about 2920, 2900 and 2870 cm^{-1} (Fig. 2b and c) were superimposed as a shoulder and shifted to the lower wavenumbers in the two AGs (Fig. 2e and f) and are assigned to the asymmetric and symmetric vibrations of aliphatic groups (CH_3 and CH_2). In all samples, we also observed skeletal vibrations of aromatic C=C (at about 1600–1520 cm^{-1}) that might be attributed to benzene, pyridine and pyrrole rings. The frequencies of pyridines are very similar to those observed in benzenes. The nitrogen atom behaves like a substituted carbon atom in benzenes. Therefore, two bands at 1940 and 1850 cm^{-1}

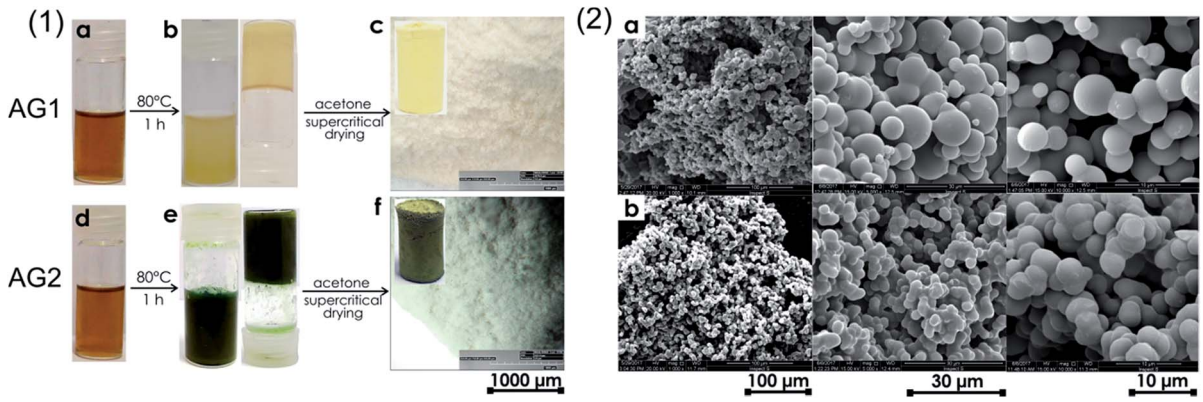

Fig. 1 (1) Photographs of (a and d) resin mixtures, (b and e) resins after aging and (c and f) optical images of aerogels from a Hirox microscope. (2) SEM images with different magnifications of (a) AG1 and (b) AG2.

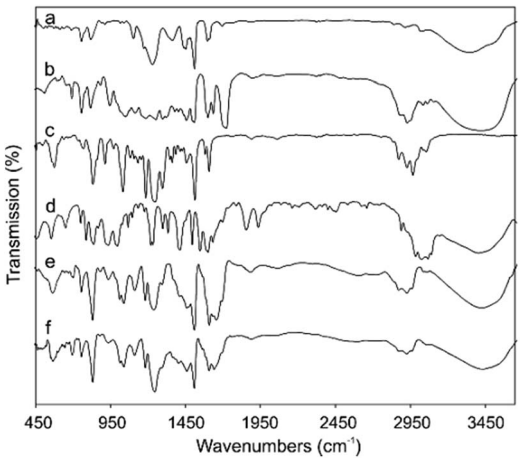

Fig. 2 ATR-FTIR spectra of (a) PhF resin, (b) PhF resin with methacrylate groups, (c) bisphenol A diglycidyl ether, (d) 4-vinylpyridine, (e) AG1 and (f) AG2.

in Fig. 2d may determine monosubstitution in 6-membered aromatic rings. The most intense bands visible at 1220, 1030, 830, and 560 cm^{-1} in the two AGs can be attributed to numerous C=C stretching, γ CH_3 and CH_2 present in polymeric networks. In the region from 1500 to 840 cm^{-1} a number of bands were observed (Fig. 2c, e and f) suggesting the presence of alcohols, ethers and related compounds in the AGs. The bands in the ranges of 1500–1350 cm^{-1} and 1100–100 cm^{-1} can be assigned to the stretching and deformation vibrations of C–O, respectively.[19] The band at 1300 cm^{-1} is due to asymmetric C–O–C stretching vibrations (Fig. 2c). The bands at 1260 and 840 cm^{-1} are characteristic of cyclic ethers, while the next two bands at 1190 and 1040 cm^{-1} are assigned to noncyclic ethers, like C=C–O-aliphatic or aromatic-C–O-aliphatic, respectively. These bands with similar wavenumbers are present in both AGs (Fig. 2e and f).

Solid-state ^{13}C CP (cross-polarization) and ^{1}H MAS NMR spectra were acquired to verify the chemical structure of the aerogels studied. The ^{13}C CP MAS NMR spectrum shown in Fig. 3(P2) revealed several signals with labelled chemical shifts and a family of spinning side-bands denoted by asterisks. The spectra of the two AGs are essentially similar as the samples did not show any significant differences in their chemical compositions. The AG1 and AG2 depicted in Fig. 3(P1) revealed a few broad, overlapping ^{1}H signals. The spectrum of AG2 was deconvoluted in terms of five signals (Fig. S1†), with the full width at half maximum ranging from 2 to 5.1 ppm (Fig. S1†). The chemical shifts of the signals and their content in the sample are listed in Table S2.† The weak signal (2.3%) at 13.4 ppm can be assigned to the protons of carboxyl groups –COOH and hydrogen bonding. The strongest signal at 1.8 ppm (36.1%) is due to the aliphatic –OH groups.[33] A newly-appearing ^{1}H signal at around 5.3 ppm might be tentatively assigned to the aromatic protons of pyridine rings (Fig. 3b(P1)), while in the ^{13}C CP MAS NMR spectrum (Fig. 3b(P2)) the characteristic signals of carbon appear at about 144 ppm. Finally, the remaining

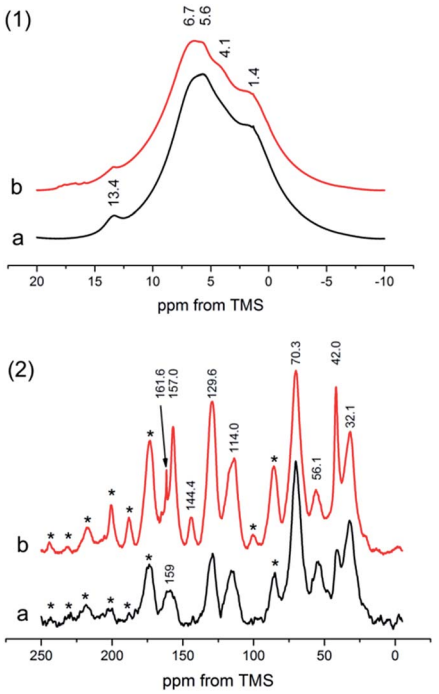

Fig. 3 (1) ^{1}H MAS NMR (MAS = 12 kHz) and (2) ^{13}C CP MAS NMR (MAS = 5.5 kHz, contact time = 2 ms) solid-state spectra of (a) AG1 and (b) AG2 samples.

signals around 7–8 ppm stem from the aromatic hydroxyl groups (Table S2†).

The ^{13}C CP MAS NMR spectra of the AG1 and AG2 samples both show characteristic signals in the aliphatic region at about 32.1 and 41 ppm ($C–CH_2–C$) and aromatic carbons in the benzene ring at 114, 129.6 and 157 ppm (Fig. 3(P2)). Finally, a strong signal at *ca.* 70 ppm is present in both ^{13}C spectra. It can be assigned to $Ar–CH_2OH$, $Ar–O–CH_2–Ar$, and $–CH_2–O–CH_2$ groups.[34]

Broadband Dielectric Spectroscopy (BDS) measurements in the frequency (f) range from 1 mHz to 1 MHz were recorded at room temperature and under ambient conditions, using a Solartron frequency response analyzer combined with a Broadband Dielectric Converter and a sample holder (Novocontrol Gmbh).[35] The frequency spectra of the real part (ε_1) of the complex permittivity (Fig. 4a) provide the values of the static

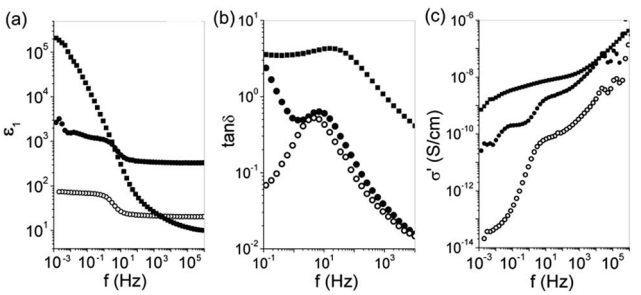

Fig. 4 Real part of complex permittivity ε_1 (a), tan δ (b) and real part of ac conductivity σ_1 *vs.* frequency *f* for OG1 (squares), AG1 (solid circles) and AG2 (doped with 4-vinylpyridine (open circles)).

dielectric constant ε_s, through the extrapolation of the low frequency plateau to the zero-frequency limit, $\varepsilon_s = 2 \times 10^5$, 103 and 70, respectively. The static dielectric constant of the AGs is lower than that of OG1, probably due to the absence of polar water molecules in the porous structure. Doping with 4-vinylpyridine suppresses the static dielectric constant of AG2. Voids, constituting the porosity, act as a network of distributed capacitors. The interaction of fluids with the internal surface area, the degree of saturation and the exchange of electrons, holes, atoms, ions or molecules among the fluid and the solid matrix, all induce changes to the capacitance of the porous network. The inflection point of $\varepsilon_1(f)$ evidences a relaxation, which can be observed clearly in the loss angle tangent tan $\delta(f)$ plots (Fig. 4b).

The peak maximum is different in the three samples; therefore, relaxation does not intrinsically occur within the bulk of the solid grains. The porous network, visualized as spatially distributed capacitors, senses the interaction of water or dopants with the inter-porous solid surface. In addition to capacitance–sensing effects (*i.e.*, ε_s and relaxation maximum changes), the dynamic ac conductivity $\sigma_1(f)$ spectra is successively suppressed by the organo to aerogel tailoring and the doping, as well.

Nowadays, with the progressive industrialization, a large number of pollutants such as organic solvents, oils, dyes and heavy metal ions are entering into water sources. Most of them are stable environmental contaminants. In this context, the search of methods for easy, efficient and low cost removal of these pollutants is strongly required. In this study, we used two organic AGs, which allow easy elimination of these pollutants *via* a convenient and low cost adsorption process. The adsorption performances of the AGs were studied and the results are shown in Fig. 5 and Table 1 (see also the ESI†).

By comparing the sorption capacity (Fig. 5 and Table 1), significant phenomena may be observed: (i) AG2 had a lower density (0.05 g cm^{-3}) compared with that of AG1 (0.08 g cm^{-3}). (ii) However, both sorbents showed a low specific surface area ($\sim$10 m^2 g^{-1}), and their mesoporous structures (BJH adsorption average pore width of 37 nm for AG1 and 30 nm for AG2) allowed efficient sorption of some organic pollutants. (iii) However, the mass-based sorption capacity is quite low for oils and organic solvents compared with other aero-sponge like materials, and they show a quick desorption rate and almost 95% removal within 5 min. (iv) The AGs show a very good recyclability due to high mechanical stability. (v) For AG1 and AG2, the adsorption capacity for MB is *ca.* 400–500 mg g^{-1} which is larger than those of the same dye with most conventional adsorbents under similar conditions (*e.g.* commercial activated carbon, 398 mg g^{-1}).

Heavy metals such as copper, manganese and iron are known to be non-biodegradable and highly toxic to environment and human health.[27,63,64] One of the efficient ways to capture heavy metal ions despite their adsorption *via* highly porous materials is introducing functional groups containing N and O as donor atoms to the structures, which are capable of forming a coordination complex with different metal ions. In this regard, pyridine

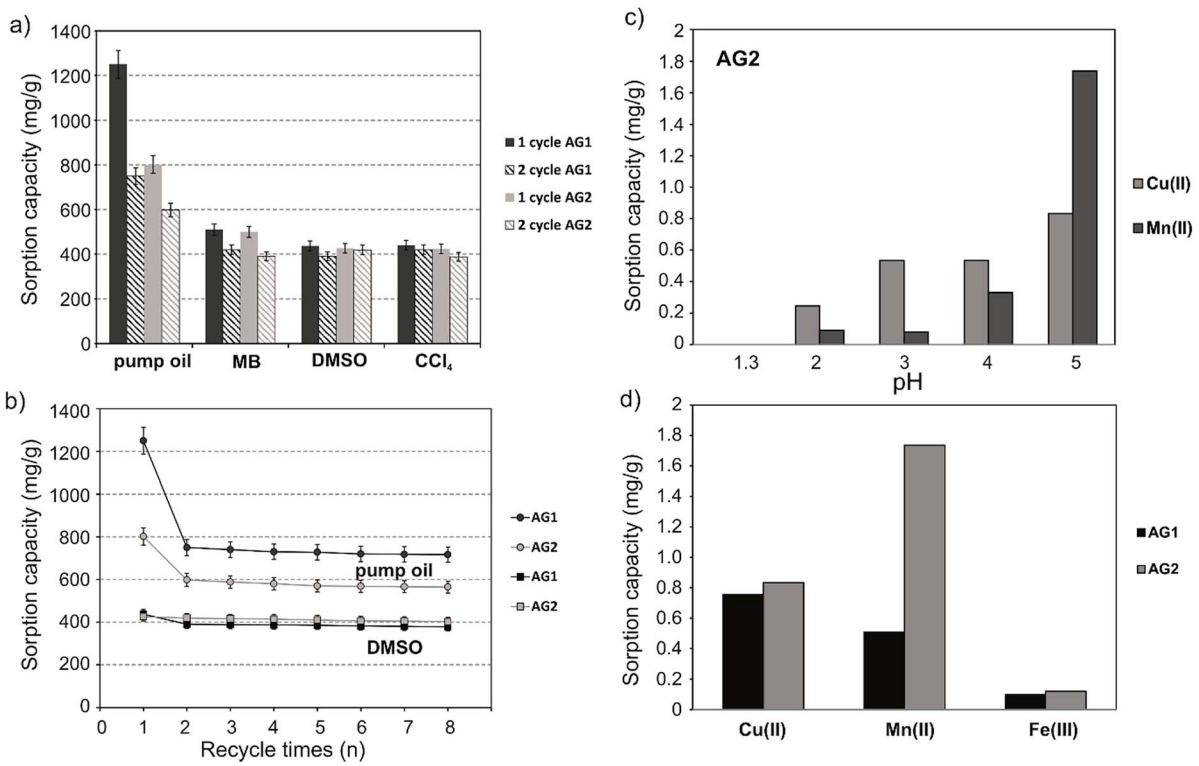

Fig. 5 Sorption capacity of AG1 and AG2 in the presence of (a) pump oil, methylene blue (MB), DMSO, and CCl_4, (b) pump oil and DMSO, (c) Cu(II) and Mn(II) at different pH values, and (d) Cu(II) and Mn(II) in HNO_3 solution at pH = 5 and Fe(III) in HNO_3 solution at pH = 2.

Table 1 Comparison of various sorbent aero-like materials for oils, organics and heavy metal ions

Substances	Type of sorbent	Sorption capacity (mg g^{-1})	Recyclability[c] (%)	Recovery method	Extraction time (h)	Ref.
Oils	AG1	750[a]–1250[b]	96[d]	Solvent extraction	1	This study
	AG2	600[a]–800[b]	94[d]	Solvent extraction	1	This study
	TCF AG	190 000	55	Combustion/squeezing	—	36
	BN-doped AG	10 times its own weight	—	—	—	37
	CNF sponges	120 000[e]	70	Mechanical squeezing	—	38
	Carbon spheres	2000 ÷ 2900	>99	Burning	—	39
	Melamine sponge	~110 000	99	Burning	—	40
	Anisotropic graphene AG	<200 times its own weight	95	Burning	—	41
	Carbon-based AG	16 times its own weight	97	Combustion/squeezing	—	42
	TiO_2/PU AG	20 000	90	Mechanical squeezing	—	43
	PU AG	45 times its own weight	—	Petroleum ether rinse	—	44
	Polyester AG	Max 3 times its own weight	—		—	45
MB	AG1	420[a]–510[b]	>85[d]	Solvent extraction	1	This study
	AG2	390[a]–500[b]	>80[d]	Solvent extraction	1	This study
	LDH + GO AG	96–125	—	—	—	46
	Graphene–MWCNT AG	190	—	Burning	10	47
	Cotton-derived CAG	<1500	—	—	—	48
	Silica–PEG AG	101.55	94.9	Burning	2	49
	Commercial activated C	398	—	Burning	—	50
DMSO	AG1	390[a]–440[b]	97[d]	Solvent extraction	1	This study
	AG2	420[a]–430[b]	96[d]	Solvent extraction	1	This study
	CNF sponges	30 000	—	Mechanical squeezing	—	51
	Microfibrillated cellulose AG	200 000	—	—	—	52
	PVA AG	140 000	87	—	—	53
	PVA–GA AG	8000	—	—	—	54
CCl_4	AG1	420[a]–440[b]	95[d]	Solvent extraction	1	This study
	AG2	390[a]–420[b]	96[d]	Solvent extraction	1	This study
	NGOA, NGA	60 000	96	Burning	—	55
	N-doped carbon AG	14 times its own weight	61	Combustion/distillation	—	56
	PVA/CNF AGs	96 000	—	—	—	57
	Carbon-based AG	26 times its own weight	97	Combustion/squeezing	—	42
	TiO_2/PU AG	43 500	90	Mechanical squeezing	—	43
	PU AG	96 times its own weight	—	Heating at 80 °C	—	44
	PVA	20 000	87	—	—	53
Cu(II)	AG1	0.754	—	—	1	This study
	AG2	0.833	—	—	1	This study
	Polybenzoxazine AG	1.501	~60	H_2O/NaCl, temperature	24	58
	Alginate AG beans	113.05	—	—	48	59
	Silane-coated PVA/CNF AG	151.3	—	—	72	57
	Graphene–MWCNT AG	9.8–33	—	—	—	47
	Chitosan AG	35.08	87	Distillation	—	21
	GO and silica AG	19	—	—	<1	60 and 61
Mn(II)	AG1	0.506	—	—	1	This study
	AG2	1.736	—	—	1	This study
	Carbon AG	1.270	Below 80	—	24	62
Fe(II)	AG1	0.099	—	—	1	This study
	AG2	0.119	—	—	1	This study

[a] Sorption capacity after 8 cycles. [b] Sorption capacity after 1 cycle. [c] Calculated recyclability after 8 cycles. [d] Calculated recyclability without the 1st cycle. [e] Absorbed oil easily poured out from the AG structure after the oil sorption test; TCF – twisted carbon fiber; CNF – cellulose nanofibril; PU – polyurethane; LDH – nanoscale layered double hydroxides; GO – graphene oxide; CAG – carbonaceous AG; PEG – polyethylene glycol; PVA – polyvinyl alcohol; GA – glutaraldehyde; NGOA – N-doped GO aerogel; NGA – N-doped graphene aerogel; MWCNT – multiwalled carbon nanotubes; MB – methylene blue; DMSO – dimethyl sulfoxide.

rings, aliphatic and aromatic hydroxyl, and epoxy modified precursors were applied for AG formation, which results in electron-donating properties of the polymeric networks. Therefore, it was also found that the presence of C=O, C–OH and C–O groups has affected the removal of these metals ions during water treatment.[65] The pyridine-like sites enable the coordination of heavy metal ions from the water sources.[65]

We have studied the possibility of using aerogels as a sorbent for the removal of heavy metals (Cu(II), Mn(II) and Fe(III)) from contaminated water sources at optimized process parameters such as pH and contact time. The experiments on Cu(II) and Mn(II) ion adsorption were carried out at different pH values corresponding to the stability of heavy metals in aqueous solutions (Fig. 5c, Table S3†). Measurements of Fe(III) were

carried out at pH 2. Experiments at higher pH values could not be performed with Fe(III) because of rapid precipitation at pH $\geq$ 2.5.

The variation in the percentage removal of Mn(II) and Cu(II) with contact time shows that all of cationic metal uptake takes place within the first 20–60 minutes (Fig. 5Sb†). It was observed that the percentage removal of studied heavy metal ions was higher on AG2 (31% Cu(II), 17% Mn(II), and 4% Fe(III)) than on AG1 (25% Cu(II), 5% Mn(II), and 3% Fe(III)).

Adsorption processes were conducted by using batch techniques for 1 hour at room temperature using 0.03 g of aerogel and 2 mL of a solution containing 150 mg L^{-1} of Mn(II) and 45 mg L^{-1} of Cu(II) and Fe(III), respectively. The concentrations of copper, iron and manganese in all tested solutions before and after sorption tests were measured under optimized conditions by flame atomic absorption spectroscopy (FAAS). To evaluate the adsorption characteristics of aerogels towards heavy metal ions, the aerogels' sorption capacity (Q, mg g^{-1}) was calculated using the formula below:

$$Q = \frac{(C_0 - C_e)V}{W} \quad (1)$$

where C_0 – initial metal ion concentration in solution (mg L^{-1}), C_e – final (residual) metal ion concentration in solution (mg L^{-1}), V – volume of the medium (L), and W – mass of the aerogel (g).

The data obtained from the studies are shown in Fig. 5c and d and Table 1. The initial study of adsorption capacities of both materials indicates their potential for the removal of the heavy metals from aqueous solutions in the order Cu(II) > Mn(II) > Fe(III) on AG1 and Mn(II) > Cu(II) > Fe(III) on AG2.

We did not observe any efficient sorption of Fe(III) *via* AG1 and AG2 (Fig. 5d). Few parameters were crucial for the removal of inorganic contaminants: charge of ions, size of their radius connected with the porous characteristics of AGs and complex formation of metals with –OH and nitrogen from pyridine rings.[65] The process of removal of metal ions from the solution was based mainly on a surface adsorption mechanism and complex formation. The first process was dominant using AG1 as a sorbent for removing Cu(II). Both processes had an impact when AG2 was applied for removing Mn(II). It was already observed that alcoholic hydroxyl groups are able to form coordinate bonds even at pH $\sim$ 5,[66] and nitrogen in the pyridine ring may constitute binding sites for copper(II) and manganese(II) ions.[65,67]

One parameter of high importance of the sorbents is their stability in strongly acidic or basic solutions. The morphologies of the AGs before and after treatment with acids and alkalis were also observed by SEM, and the results showed some changes in the microstructures of the AGs (Fig. S3 and S4†) suggesting that a longer contact time with concentrated acid or alkali solutions leads to the gradual destruction of AGs.

Table 1 gives an overview regarding the effectiveness of the state-of-the-art adsorbents with regard to their sorption performance towards organics, oils and heavy metal ions. According to the literature, the major disadvantages regarding the aero-like materials are their poor biodegradability, low selectivity, poor floatability and slow kinetics.[1] In addition, many of them are characterized by poor mechanical strength.[1] Despite these properties they show higher sorption capacity for oils and other toxic organic compounds from water compared with conventional sorbents. In recent years, particular attention has been paid to the development of 3D carbon-based AGs.[1,3,36,39,55,68] Owing to their unusual properties, such as high porosity, low density, large specific surface area, and high microporosity and surface hydrophobicity, they are recognized as excellent oil and organic solvent sorbents. It has to be underlined that this type of AG usually shows low mechanical stability. The answer to these problems is the synthesis of composite AGs[30,43,69] with a better mechanical compressibility and hydrophobicity that resulted from the synergetic effect of their components.

It has to be underlined that phenol-formaldehyde AGs have a good sorption capacity towards Cu(II) and Mn(II) ions in comparison to other porous sorbents. The AGs also showed good sorption properties towards organic solvents and methylene blue. Presently, our study aims to improve the sorption and structural properties of AGs by using pyrolysis processes. This method will allow the creation of 3D carbonaceous frameworks, which may have a lower density, higher values of specific surface area and microporosity. Although the organic AGs may lose their selectivity after transformation to carbon-based networks, it should definitely improve the analytical parameters, including sorption capacity towards organic solvents and oils, due to optimization of textural parameters and increasing their hydrophobicity.

Conclusions

In conclusion, we have demonstrated the first example of phenol-formaldehyde-based aerogels used in the removal of oils, organics and heavy metal ions from wastewater. The nanoporous structures of AGs can be tuned by the concentration of used monomers. Despite the fact that PhF organic AGs show lower sorption capacity compared to some other aero-like sorbents, AG1 and AG2 are still promising to be used for removing some organic pollutants and heavy metal ions from wastewater, considering the multifunctionality, low-cost, fast sorption rate and excellent recyclability. BDS results indicate that the huge internal grain surface areas of AGs exhibit increased efficiency of collecting undesirable atoms or molecules by transferring them through the porous system by fluids or air. Aerogels may also be used as sensors of such entities by simply recording changes, of some orders of magnitude, in both the capacitance and electric conductivity.

Conflicts of interest

There are no conflicts to declare.

Acknowledgements

We gratefully acknowledge the financial support of the Ministry of Science and Higher Education, Poland to M. E. P.-B, B. S.

gratefully acknowledges Ministry of Science and Higher Education for the solid-state NMR 500 MHz spectrometer investment Grant (project No. 75/E-68/S/2008-2). SEM and FTIR were funded by European Funds for Regional Development and National Funds of Ministry of Science and Higher Education, as part of the Operational Programme Development of Eastern Poland 2007–2013, projects: POPW.01.03.00-20-034/09 and POPW.01.03.00-20-004/11.

Notes and references

1 H. Maleki, *Chem. Eng. J.*, 2016, **300**, 98–118.
2 S. M. Tehrani, Y. Lu and M. A. Winnik, *Macromolecules*, 2016, **49**, 8711–8721.
3 Z.-Y. Wu, H.-W. Liang, L.-F. Chen, B.-C. Hu and S.-H. Yu, *Acc. Chem. Res.*, 2016, **49**, 96–105.
4 S.-M. Alatalo, F. Pileidis, E. Mäkilä, M. Sevilla, E. Repo, J. Salonen, M. Sillanpää and M.-M. Titirici, *ACS Appl. Mater. Interfaces*, 2015, **7**, 25875–25883.
5 J. Zheng, S. Jung, P. W. Schmidt, T. P. Lodge and T. M. Reineke, *ACS Macro Lett.*, 2017, **6**, 145–149.
6 V. Chabot, D. Higgins, A. Yu, X. Xiao, Z. Chen and J. Zhang, *Energy Environ. Sci.*, 2014, **7**, 1564.
7 J. Wang, X. Wang and X. Zhang, *J. Mater. Chem. A*, 2017, **5**, 4308–4313.
8 L. Chen, X. Wang, X. Zhang and H. Zhang, *J. Mater. Chem.*, 2012, **22**, 22090.
9 J. Stergar and U. Maver, *J. Sol-Gel Sci. Technol.*, 2016, **77**, 738–752.
10 Y. Qian, I. M. Ismail and A. Stein, *Carbon*, 2014, **68**, 221–231.
11 R. W. Pekala, *J. Mater. Sci.*, 1989, **24**, 3221–3227.
12 J. Biener, M. Stadermann, M. Suss, M. A. Worsley, M. M. Biener, K. A. Rose and T. F. Baumann, *Energy Environ. Sci.*, 2011, **4**, 656.
13 S. A. Al-Muhtaseb and J. A. Ritter, *Adv. Mater.*, 2003, **15**, 101–114.
14 H. Cheng, H. Xue, C. Hong and X. Zhang, *Compos. Sci. Technol.*, 2017, **140**, 63–72.
15 D. R. Rolison, J. W. Long, J. C. Lytle, A. E. Fischer, C. P. Rhodes, T. M. McEvoy, M. E. Bourg and A. M. Lubers, *Chem. Soc. Rev.*, 2009, **38**, 226–252.
16 S. Mahadik-Khanolkar, S. Donthula, C. Sotiriou-Leventis and N. Leventis, *Chem. Mater.*, 2014, **26**, 1303–1317.
17 J. Wang and X. Zhang, *ACS Nano*, 2015, **9**, 11389–11397.
18 Z.-L. Yu, G.-C. Li, N. Fechler, N. Yang, Z.-Y. Ma, X. Wang, M. Antonietti and S.-H. Yu, *Angew. Chem., Int. Ed.*, 2016, **55**, 14623–14627.
19 Q. Fang, X. Zhou, W. Deng and Z. Liu, *Chem. Eng. J.*, 2017, **308**, 1001–1009.
20 B. J. Riley, J. Chun, J. V. Ryan, J. Matyáš, X. S. Li, D. W. Matson, S. K. Sundaram, D. M. Strachan and J. D. Vienna, *RSC Adv.*, 2011, **1**, 1704.
21 A. Li, R. Lin, C. Lin, B. He, T. Zheng, L. Lu and Y. Cao, *Carbohydr. Polym.*, 2016, **148**, 272–280.
22 B. Vivek and E. Prasad, *ACS Appl. Mater. Interfaces*, 2017, **9**, 7619–7628.
23 I. R. Pala and S. L. Brock, *ACS Appl. Mater. Interfaces*, 2012, **4**, 2160–2167.
24 Z. Huang, L. Lu, Z. Cai and Z. J. Ren, *J. Hazard. Mater.*, 2016, **302**, 323–331.
25 P. Rana-Madaria, M. Nagarajan, C. Rajagopal and B. S. Garg, *Ind. Eng. Chem. Res.*, 2005, **44**, 6549–6559.
26 Y. Xu, Z. Sui, B. Xu, H. Duan and X. Zhang, *J. Mater. Chem.*, 2012, **22**, 8579.
27 R. K. Gautam, S. K. Sharma, S. Mahiya and M. C. Chattopadhyaya, in *Heavy Metals In Water*, ed. S. Sharma, Royal Society of Chemistry, Cambridge, 2014, pp. 1–24.
28 L. F. Dumée, Z. Yi, B. Tardy, A. Merenda, E. des Ligneris, R. R. Dagastine and L. Kong, *Sci. Rep.*, 2017, **7**, 45112.
29 Z. Hou, Y. Jin, X. Xi, T. Huang, D. Wu, P. Xu and R. Liu, *J. Colloid Interface Sci.*, 2017, **488**, 317–321.
30 L. Zuo, Y. Zhang, L. Zhang, Y.-E. Miao, W. Fan and T. Liu, *Materials*, 2015, **8**, 6806–6848.
31 H. Pan, *Renewable Sustainable Energy Rev.*, 2011, **15**, 3454–3463.
32 M. Bozlar, C. Punckt, S. Korkut, J. Zhu, C. Chiang Foo, Z. Suo and I. A. Aksay, *Appl. Phys. Lett.*, 2012, **101**, 091907.
33 E. Pretsch, P. Buhlmann and M. Badertscher, *Structure Determination of Organic Compounds*, ed. E. Pretsch, Springer Berlin Heidelberg, Berlin, Heidelberg, 2009.
34 G. E. Maciel, I. S. Chuang and L. Gollob, *Macromolecules*, 1984, **17**, 1081–1087.
35 C. Lampadaris, I. Sakellis and A. N. Papathanassiou, *Appl. Phys. Lett.*, 2017, **110**, 222901.
36 H. Bi, Z. Yin, X. Cao, X. Xie, C. Tan, X. Huang, B. Chen, F. Chen, Q. Yang, X. Bu, X. Lu, L. Sun and H. Zhang, *Adv. Mater.*, 2013, **25**, 5916–5921.
37 Y. Liu, M. Xiang and L. Hong, *RSC Adv.*, 2017, **7**, 6467–6473.
38 O. Laitinen, T. Suopajärvi, M. Österberg and H. Liimatainen, *ACS Appl. Mater. Interfaces*, 2017, **9**, 25029–25037.
39 Y. Feng, S. Liu, G. Liu and J. Yao, *Chemosphere*, 2017, **170**, 68–74.
40 W. Zhang, X. Zhai, T. Xiang, M. Zhou, D. Zang, Z. Gao and C. Wang, *J. Mater. Sci.*, 2017, **52**, 73–85.
41 T. Liu, M. Huang, X. Li, C. Wang, C.-X. Gui and Z.-Z. Yu, *Carbon*, 2016, **100**, 456–464.
42 S. Han, Q. Sun, H. Zheng, J. Li and C. Jin, *Carbohydr. Polym.*, 2016, **136**, 95–100.
43 Q. Shuai, X. Yang, Y. Luo, H. Tang, X. Luo, Y. Tan and M. Ma, *Mater. Chem. Phys.*, 2015, **162**, 94–99.
44 P. Xi, L. Huang, Z. Xu, F. Chen, L. An, B. Wang and Z.-N. Chen, *RSC Adv.*, 2014, **4**, 59481–59485.
45 L. Wu, J. Zhang, B. Li and A. Wang, *J. Colloid Interface Sci.*, 2014, **413**, 112–117.
46 Q. Fang and B. Chen, *J. Mater. Chem. A*, 2014, **2**, 8941–8951.
47 Z. Sui, Q. Meng, X. Zhang, R. Ma and B. Cao, *J. Mater. Chem.*, 2012, **22**, 8767.
48 H. Chen, X. Wang, J. Li and X. Wang, *J. Mater. Chem. A*, 2015, **3**, 6073–6081.

49 P. S. Suchithra, L. Vazhayal, A. Peer Mohamed and S. Ananthakumar, *Chem. Eng. J.*, 2012, **200–202**, 589–600.
50 W. Li, Z. Zhang, B. Kong, S. Feng, J. Wang, L. Wang, J. Yang, F. Zhang, P. Wu and D. Zhao, *Angew. Chem., Int. Ed.*, 2013, **52**, 8151–8155.
51 A. Mulyadi, Z. Zhang and Y. Deng, *ACS Appl. Mater. Interfaces*, 2016, **8**, 2732–2740.
52 S. Zhou, P. Liu, M. Wang, H. Zhao, J. Yang and F. Xu, *ACS Sustainable Chem. Eng.*, 2016, **4**, 6409–6416.
53 Y. Pan, W. Wang, C. Peng, K. Shi, Y. Luo and X. Ji, *RSC Adv.*, 2014, **4**, 660–669.
54 Y. Pan, C. Peng, W. Wang, K. Shi, Z. Liu and X. Ji, *RSC Adv.*, 2014, **4**, 35620–35628.
55 H. Ren, X. Shi, J. Zhu, Y. Zhang, Y. Bi and L. Zhang, *J. Mater. Sci.*, 2016, **51**, 6419–6427.
56 Y. Yang, Z. Tong, T. Ngai and C. Wang, *ACS Appl. Mater. Interfaces*, 2014, **6**, 6351–6360.
57 Q. Zheng, Z. Cai and S. Gong, *J. Mater. Chem. A*, 2014, **2**, 3110.
58 T. Chaisuwan, T. Komalwanich, S. Luangsukrerk and S. Wongkasemjit, *Desalination*, 2010, **256**, 108–114.
59 E. G. Deze, S. K. Papageorgiou, E. P. Favvas and F. K. Katsaros, *Chem. Eng. J.*, 2012, **209**, 537–546.
60 X. Mi, G. Huang, W. Xie, W. Wang, Y. Liu and J. Gao, *Carbon*, 2012, **50**, 4856–4864.
61 S. Štandeker, A. Veronovski, Z. Novak and Ž. Knez, *Desalination*, 2011, **269**, 223–230.
62 A. K. Meena, G. K. Mishra, P. K. Rai, C. Rajagopal and P. N. Nagar, *J. Hazard. Mater.*, 2005, **122**, 161–170.
63 R. Singh, N. Gautam, A. Mishra and R. Gupta, *Indian J. Pharmacol.*, 2011, **43**, 246.
64 M. Jaishankar, T. Tseten, N. Anbalagan, B. B. Mathew and K. N. Beeregowda, *Interdiscip. Toxicol.*, 2014, **7**, 60–72.
65 F. Dwyer, *Chelating Agents and Metal Chelates*, Academic Press, New York, London, 1964.
66 Y. Shao and J. Chen, *J. Solution Chem.*, 2009, **38**, 1357–1367.
67 N. A. Rey, K. C. dos Santos, M. Â. B. C. Menezes, A. S. Mangrich and E. C. Pereira-Maia, *J. Braz. Chem. Soc.*, 2006, **17**, 497–504.
68 P. Hu, B. Tan and M. Long, *Nanotechnol. Rev.*, 2016, **5**, 23–29.
69 S. Zhou, G. Hao, X. Zhou, W. Jiang, T. Wang, N. Zhang and L. Yu, *Chem. Eng. J.*, 2016, **302**, 155–162.